Deep eutectic solvents based on N-methylacetamide and a lithium salt as suitable electrolytes for lithium-ion batteries

PCCP

RSC Publishing

PAPER

View Article Online
View Journal | View Issue

Cite this: *Phys. Chem. Chem. Phys.*, 2013, **15**, 20054

Deep eutectic solvents based on *N*-methylacetamide and a lithium salt as suitable electrolytes for lithium-ion batteries

Aurélien Boisset,[a] Sebastian Menne,[b] Johan Jacquemin,[c] Andrea Balducci[b] and Mérièm Anouti*[a]

Received 10th August 2013,
Accepted 3rd October 2013

DOI: 10.1039/c3cp53406e

www.rsc.org/pccp

In this work, we present a study on the physical and electrochemical properties of three new Deep Eutectic Solvents (DESs) based on *N*-methylacetamide (MAc) and a lithium salt (LiX, with X = bis[(trifluoromethyl)sulfonyl]imide, TFSI; hexafluorophosphate, PF_6; or nitrate, NO_3). Based on DSC measurements, it appears that these systems are liquid at room temperature for a lithium salt mole fraction ranging from 0.10 to 0.35. The temperature dependences of the ionic conductivity and the viscosity of these DESs are correctly described by using the Vogel–Tammann–Fulcher (VTF) type fitting equation, due to the strong interactions between Li^+, X^- and MAc in solution. Furthermore, these electrolytes possess quite large electrochemical stability windows up to 4.7–5 V on Pt, and demonstrate also a passivating behavior toward the aluminum collector at room temperature. Based on these interesting electrochemical properties, these selected DESs can be classified as potential and promising electrolytes for lithium-ion batteries (LIBs). For this purpose, a test cell was then constructed and tested at 25 °C, 60 °C and 80 °C by using each selected DES as an electrolyte and $LiFePO_4$ (LFP) material as a cathode. The results show a good compatibility between each DES and LFP electrode material. A capacity of up to 160 mA h g^{-1} with a good efficiency (99%) is observed in the DES based on the $LiNO_3$ salt at 60 °C despite the presence of residual water in the electrolyte. Finally preliminary tests using a LFP/DES/LTO (lithium titanate) full cell at room temperature clearly show that LiTFSI-based DES can be successfully introduced into LIBs. Considering the beneficial properties, especially, the cost of these electrolytes, such introduction could represent an important contribution for the realization of safer and environmentally friendly LIBs.

1. Introduction

Developing new and safer solvents is one of the key subjects in Green Chemistry. Ionic liquids (ILs) and deep eutectic solvents (DESs), thus, have been paid great attention to replace current organic solvents and have been applied to many chemical processes. It is a well-known phenomenon that pure solid chemicals can become liquid by mixing in certain ratios as in the case of DESs, which are made by mixing a quaternary ammonium salt with a metal salt,[1] a hydrated salt[2] or a simple hydrogen bond donor (HDB) such as alcohol, amide and carboxylic acid[3,4] as a complexing agent. This results in the formation of an eutectic mixture with a melting point temperature that is considerably lower than its original precursors mainly due to the generation of intermolecular hydrogen bonds. We demonstrate in a recent paper[5] that *N*-methylacetamide can be considered to be a good and green solvent for the formulation of new DES-based electrolytes able to decrease the melting point of a complex system containing a molten salt due to its "water-like" physical properties (*e.g.* very high dielectric constant (ε = 178.9), high dipolar moment μ = 6.8 D, and very low vapor pressure p_{vap} = 0.050 kPa at 40 °C).[6] These DESs have physical properties and phase behavior similar to that of classical ILs.[7] However, compared to the broad applications of ILs,[8–11] the application of DESs has been so far limited to organic reactions[12–16] and electrodeposition.[17] The main advantages of DESs in comparison with ILs are the extremely low cost of their precursors and their general biodegradability. Like ILs, DESs have some interesting and tailored properties – such as high conductivity, large mutual solubility with metal salts, wide potential windows and the absence of secondary reaction like water electrolysis as compared with organic or non-aqueous solvents – which make them suitable as electrolytes for electrochemical processes.[18–20]

[a] *Université François Rabelais, Laboratoire PCM2E, Parc de Grandmont, 37200 Tours, France. E-mail: meriem.anouti@univ-tours.fr; Fax: +33 247367073; Tel: +33 247366951*
[b] *Westfälische Wilhelms-Universität, Institut für Physikalische Chemie-MEET, Corrensstr. 28/30, 48149 Münster, Germany*
[c] *CenTACat – School of Chemistry and Chemical Engineering, Queen's University Belfast, Belfast, Northern Ireland, UK*

However DESs are very hygroscopic, and even if the presence of water does not appear to lead to the electrolyte decomposition, it complicates the reproducible performance of measurements especially by using a non-carefully and non-controlled atmosphere. The evaluation of DESs as new generation of solvents for various practical applications requires enough knowledge of some of the main physical, chemical, and thermodynamic properties. A few research articles were recently added to the literature dealing with this topic,[21–26] yet, the door is still wide-open for more research in this area.

$LiFePO_4$ with an olivine structure has been studied extensively as a cathode material for lithium-ion batteries (LiBs) due to its main advantages such as low cost, good cycling performance at room temperature, high safety, non-toxicity and environmental friendliness. It is now popularly considered that $LiFePO_4$ has the most suitable cathode material characteristics for application in middle/large-size electric vehicle (EV) and hybrid electric vehicle (HEV) batteries. But $LiFePO_4$ also exhibits capacity fading problems during cycling at elevated temperatures due to iron dissolution as well as the occurrence in the cell of impurities such as HF and H_2O.[27–30] The presence of such impurities at elevated temperatures can promote iron dissolution of the $LiFePO_4$ surface and decompose the electrolyte, which then contributes to the formation of thick obstructive solid/electrolyte interphase (SEI) films.[31]

In the present study, some physical/chemical properties of the selected DES based on the binary mixture of lithium salt LiX (X = bis[(trifluoromethyl)sulfonyl]imide, hexafluorophosphate, and nitrate) and *N*-methylacetamide (MAc) have been investigated and compared as a function of the temperature. Firstly, the thermal properties of each investigated DES were determined by differential scanning calorimetry (DSC) to establish its binary solid–liquid equilibrium phase diagram as a function of the salt structure, composition and temperature. The ionic conductivity and the viscosity of the DESs were measured from 25 °C to 80 °C and were then discussed through Vogel–Tamman–Fulcher (VTF) equations to extract the activation energy associated with these transport properties. The knowledge of these properties as a function of the composition and temperature contributed then to the formulation of the electrolyte for the LiB applications. We finally compared the electrochemical performances of selected DESs as electrolytes for the LiB applications with the lithium iron phosphate olivine (LFP) electrode at room temperature, 60 °C and 80 °C and different water contents in the solution.

2. Experimental section

2.1. Materials

Lithium bis[(trifluoromethyl)sulfonyl]imide (LiTFSI, ≥99.0%) was obtained from Solvionic, lithium hexafluorophosphate ($LiPF_6$, >99.0%) and lithium nitrate ($LiNO_3$, >99.0%) were obtained from Sigma Aldrich. Anhydrous *N*-methylacetamide (MAc, 99.8%) was purchased from Sigma Aldrich and redistilled before any utilization.

2.2. Preparation of DESs

Each DES solution was simply prepared on mass by mixing at ambient temperature known quantities of the dried lithium salt and freshly distillated and degassed *N*-methylacetamide (MAc), giving an uncolored viscous liquid, which was stored in an argon-filled glove box Mbraun with oxygen and water contents lower than 1 ppm. The selected LiX/MAc mole ratio composition, reported here in the salt mole fraction denoted $x_{Li^+} = 1/(1 + n)$ (*e.g.* 1 mol of LiTFSI mixed into *n* mol of MAc), was stored inside the argon-filled glove box to avoid any water contamination coming from the atmosphere during the whole study. The water content in each investigated electrolyte determined by Coulometric Karl-Fischer titration was controlled to investigate the water content effect before and after any measurement during this work, the water content is found to be close to 40, 300 and 565 ppm for LiTFSI–MAC, $LiPF_6$–MAC and $LiNO_3$–MAC, respectively. This result is linked to the hydrophobic and hydrophilic nature of the $TFSI^-$ and NO_3^- anions, respectively.

2.3. Preparation of electrode material

The LFP and the LTO electrodes used for the realization of the LIBs investigated in this work were prepared using a procedure identical to that reported in ref. 32. The composition of the dried electrodes was 85% active material, 10% conductive agent and 5% binder. The geometric area of the electrodes was 1.13 cm^2. The mass loading of LFP electrodes was 1 mg cm^{-2}, while that of the LTO electrodes was 3.1 mg cm^{-2}.

2.4. Measurements

A Crison (GLP 31) digital multifrequency conductometer was utilized to measure ionic conductivities. The temperature control, from 25 to 80 °C, was realized using a JULABO F25 thermostated bath, with an accuracy of ±0.2 °C; the uncertainty for the conductivities did not exceed ±2%. Each conductivity was recorded when the stability was superior to 1% within 2 min. A TA Instruments rheometer AR 1000 was used to determine the rheological behavior and the viscosity of the DES by using a conical geometry. The temperature in the cell was automatically regulated using a solid-state thermostat (Peltier) within ±0.01 °C. The uncertainty of viscosity measurements did not exceed ±1%. Differential scanning calorimetry (DSC) was carried-out on a Perkin-Elmer DSC 4000, under a nitrogen atmosphere, coupled with an Intracooler SP VLT 100. Samples for DSC measurements were sealed in Al pans.

The electrochemical measurements were carried-out using a MACCOR Series 4000 battery tester. All tests were carried out in three-electrode Swagelok® cells at room temperature, 60 °C and 80 °C. The cells were assembled in a dry box (presenting a water content lower than 1 ppm). As a separator, a stack of three non-woven fleeces (FS2226, Freudenberg, Germany) drenched with 100 mm^3 of the electrolyte was used. The LIBs investigated in this work were all cathode limited. Therefore, all values of capacity reported in the next pages are always referred to the LFP cathode.

The optimization of 3D structure of each investigated anion and MAc was carried-out by using DFT calculations within Gaussian software (Gaussian version 03-D1, DFT-B3LYP-DGTZVP)[33,34] and then used to generate from each resultant optimized structure its COSMO file (TURBOMOLE, BP-DFT-Ahlrichs-TZVP).[35] The COSMO volume and the sigma profile of each structure were then directly obtained by using the COSMOthermX software (version 2.1, release 01.08)[36] based on the COSMO-RS (Conductor-like Screening Model for Real Solvents) model.[37,38]

3. Results and discussion

3.1. Physical properties of the DES

When a lithium salt, LiX (X = TFSI, NO_3, or PF_6), and MAc are mixed together within an appropriate molar ratio range, a homogeneous liquid mixture is obtained even at room temperature. The surface of lithium salt particles becomes wet upon contacting MAc particles, and then some liquid drops appear immediately when the mixture of LiX and MAc is mechanically stirred at room temperature. Herein, the transparent and homogeneous solutions were formed after 10 min of stirring. It is interesting to notify that two solids at room temperature (MAc T_m = 35 °C and lithium salt T_m > 200 °C) can form a homogeneous liquid at room temperature when they are mixed in a specific composition range. This behavior is similar to that of an ionic liquid in which the presence of large ions hinders the crystallization of the liquid at room temperature. In the present case, it is reasonable to assume that MAc works as a complexing agent for both cations and anions due to its two polar groups (C=O group and NHR group) capable of coordinating with cations and anions, respectively, weakening and even breaking the bonds between Li^+ cations and anions as illustrated in Scheme 1.

The strong interaction of acetamide (–CO–NH–CH_3) groups with ions (cations and anions) can lead to formation of coordinated complexes producing micro-domains in solution. This formation of micro-domains is supported by several works dealing with infrared[39] and dielectric relaxation measurements[40] which have provided an estimation of this domain size in the (amide + salt) DES. For example, Abdulnur and Laki[41] shown that the cation–MAc–anion interactions in solution result in a net residual charge on MAc, which becomes less positive as the difference in charge density between the anion and the cation of the salt increases. Authors have then calculated the optimal distance of approach for lithium cations to the oxygen atom on the MAc structure, which is close to d = 2.16 Å, and the resultant electronic charge on MAc, obtained from Mulliken population analysis, is close to Q = +0.27. Additionally, they evaluated also the interaction energy of the Li^+ with MAc to be ΔE = 346.9 kJ mol^{-1}.[41]

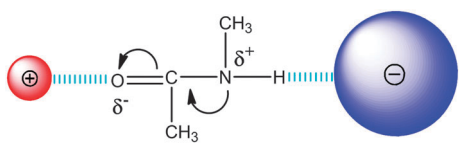

Scheme 1 Schematic representation of the cation–MAc–anion system.

In the present cases, the oxygen atom in the C=O group of MAc has a tendency to coordinate the Li^+ cations, because O atoms are negatively charged and Li^+ cations have a high capability of adsorbing electrons. The (N–H···O) hydrogen bond in the solvent structure is a central factor explaining why the MAc is solid at room temperature, while by adding a LiX salt in this solvent, the interaction between MAc and LiX weakens or even breaks this intra (N–H···O) hydrogen bond due to the competitive Li^+···O interactions in solution. At the same time, the ionic bond in LiX is a weakening process between LiX and MAc. From these considerations and according also to the volumes and sigma profiles of investigated anions and MAc reported in Table 1, it is then easy to imagine that the formation of a DES by mixing MAc with LiX is easier in the following order X = $TFSI^-$ > PF_6^- > NO_3^-.

3.1.1. Thermal properties. Fig. 1 shows the differential scanning calorimetry (DSC) curves of the LiTFSI–MAc binary system as a function of the lithium salt mole fraction, x_{Li^+}, from 0.05 to 0.50 and of the temperature from −150 to 150 °C. As shown in Fig. 1, only one endothermic peak in each DSC curve is obtained when the salt mole fraction x_{Li^+} is ranged from 0.35 to 0.50.

However, two endothermic peaks can be observed in the samples beyond a mole fraction composition of 0.25, which clearly indicate the existence of the liquid–solid coexistence regime between the eutectic temperature (−72 °C) and the liquidus curve. Furthermore, most of these DSC curves show also an exothermic peak, which is a devitrification temperature (T_d) (see for example the green curve at x_{Li^+} = 0.25 in Fig. 1), as already mentioned for similar systems.[42,43]

Using thermal properties reported in Fig. 1, the solid–liquid equilibrium phase diagram of the LiTFSI–MAc mixture was then constructed, as shown in Fig. 2.

This phase diagram displays the typical eutectic character of the LiTFSI–MAc mixture, having an eutectic point localized at an eutectic temperature of −72 °C (201 K) and a lithium salt mole fraction close to 0.20. Similar fluid phase behavior in the case of the LiTFSI and acetamide mixture has been previously reported.[39] Fig. 2 represents the solid–liquid equilibrium of the MAc–LiTFSI binary mixture as a function of the salt molar fraction, x_{Li^+}, with an eutectic temperature of around −72 °C. We finally notify that the slight inclination of the eutectic plateau (Fig. 2) between the solid phase and the liquid, MAc + LiX mixtures and liquid, is probably due to the presence of water (285 ppm) that modifies the behavior of solid–liquid properties of neat mixtures as the LiX–MAc ones.

Similarly, DSC measurements were also performed to explore the thermal properties of the $LiPF_6$–MAc and $LiNO_3$–MAc mixtures. Based on this work, it was observed that all DSC thermograms of selected mixtures have a nearly constant endothermic peak corresponding to the eutectic temperature of selected DES mixtures, which is close to T_e = −52 °C at x_{Li^+}, close to 0.16, and close to T_e = −75 °C at x_{Li^+}, close to 0.30 in the

Table 1 Structures, COSMO volumes and sigma profiles of studied anion (X^-) in lithium salt LiX and of the *N*-methylacetamide

Structure/COSMO volume (Å^3)	Sigma profile
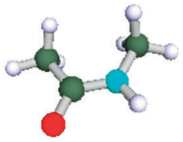 MAc (101.2)	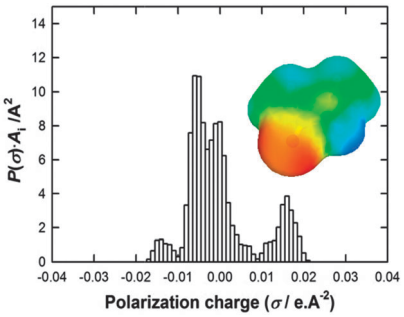
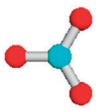 NO_3 (56.7)	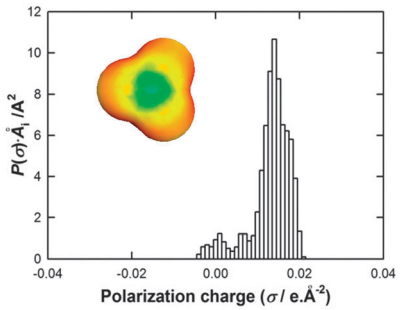
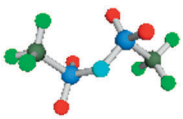 TFSI (219.4)	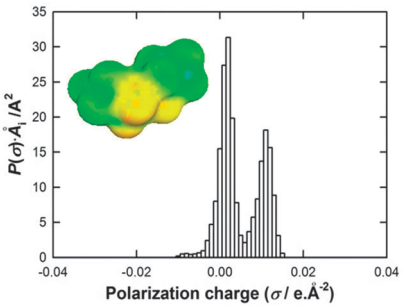
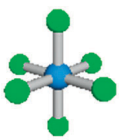 $LiPF_6^-$ (103.7)	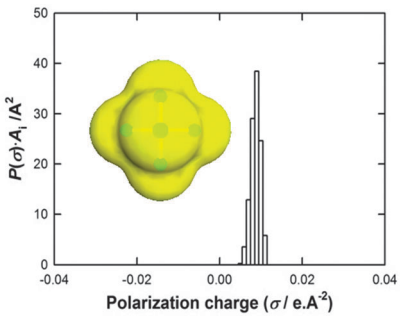
	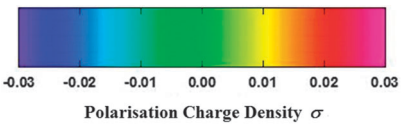

Polarisation Charge Density σ

case of the $LiPF_6$–MAc and $LiNO_3$–MAc mixtures, respectively. As presented in Table 2, all systems present eutectic points lower than −50 °C, indicating the existence of the strong interaction between each lithium salt and MAc, as previously discussed. A lithium mole fraction of 0.20 has been chosen for

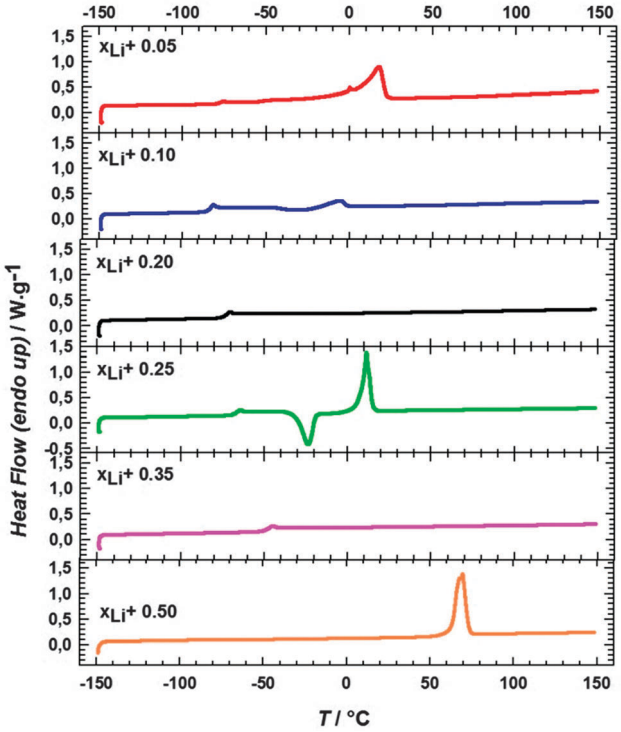

Fig. 1 The DSC curves of LiTFSI–MAc mixtures as a function of the salt molar fraction, x_{Li^+}.

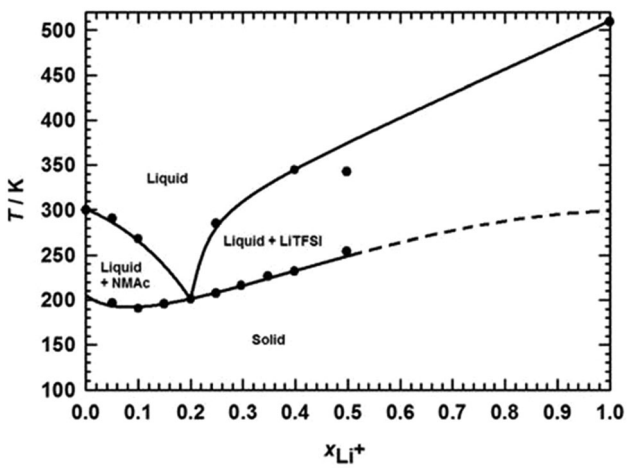

Fig. 2 Solid–liquid equilibrium of the MAc–LiTFSI binary mixture as a function of the salt mole fraction, x_{Li^+} describing a typical DES thermal behavior.

Table 2 Conductivity and viscosity of selected DESs at a lithium salt mole fraction x_{Li^+} = 0.20 at various temperatures. T_e values are eutectic points

		Ionic conductivity (mS cm^{-1})			Viscosity (mPa s)		
DES mixture	T_e (°C)	25 °C	60 °C	80 °C	25 °C	60 °C	80 °C
LiTFSI–MAc	−72	1.35	5.59	9.22	78.38	22.15	14.20
$LiNO_3$–MAc	−75	0.76	3.25	6.30	107.19	23.31	12.14
$LiPF_6$–MAc	−52	1.41	5.86	10.13	nd	34.22	19.73

physical and electrochemical characterization of each DES. The phenomenon observed during the sample preparation and the

DSC results clearly indicate that eutectic systems, liquids at room temperature, can be formed by mixing selected LiX salts with the *N*-methylacetamide.

3.1.2. Transport properties of the PIL

Conductivity. The conductivity of electrolyte solutions of LiTFSI–MAc and $LiPF_6$–MAc (at x_{Li^+} = 0.20) was measured between 20 °C and 80 °C, and the results are shown in Fig. 3 and Table 2. As expected, the conductivity of these DESs increases with the temperature from 1.20 mS cm^{-1} and 1.35 mS cm^{-1} at 20 °C and reaches 9.22 mS cm^{-1} and 10.13 mS cm^{-1} at 80 °C for LiTFSI–MAc and $LiPF_6$–MAc mixtures, respectively. At 25 °C, the conductivity of the LiTFSI–MAc system at x_{Li^+} = 0.20 is close to that reported by Chen *et al.*[44] for the LiTFSI–Acetamide mixture (*e.g.* 1.26 mS cm^{-1}), showing that the presence of an extra methyl group on the structure of the solvent does not seem to affect this transport property, such a value is more than six times higher than that reported for $LiPF_6$ and acetamide at the same salt mole fraction and temperature (*e.g.* at x_{Li^+} = 0.20 and 25 °C, σ = 0.2 mS cm^{-1}).[45]

Additionally, Fig. 4a clearly shows that the variation of $\ln(\sigma)$ as a function of $(1/T)$ is not a linear function (eqn (1)), we can then conclude that the two systems do not show an Arrhenius behavior, and the Vogel–Tamman–Fulcher equation (eqn (2)) was used to determine the temperature dependence of the conductivity.

$$\sigma = \sigma_0 \exp\left[\frac{-E_a}{T}\right] \quad (1)$$

$$\sigma = \sigma_0 \exp\left[\frac{-B_1'}{T - T_0}\right] \quad (2)$$

here, σ_0 (mS cm^{-1}), B_1 (K), and T_0 (K) are fitting parameters. The product B_1R (where R is the molar gas constant) has the dimension of the activation energy (kJ mol^{-1}). Fig. 4b represents the VTF plot. According to eqn (2), fitting parameters can be determined for the studied DES systems and are presented herein in Table 3. We can observe that pseudo-activation energy for conductivity and viscosity is more than 2 times higher for the $LiNO_3$–MAc system than for the $LiPF_6$–MAc, indicating a larger effect of temperature dependence on transport mechanisms for the $LiNO_3$ based system.

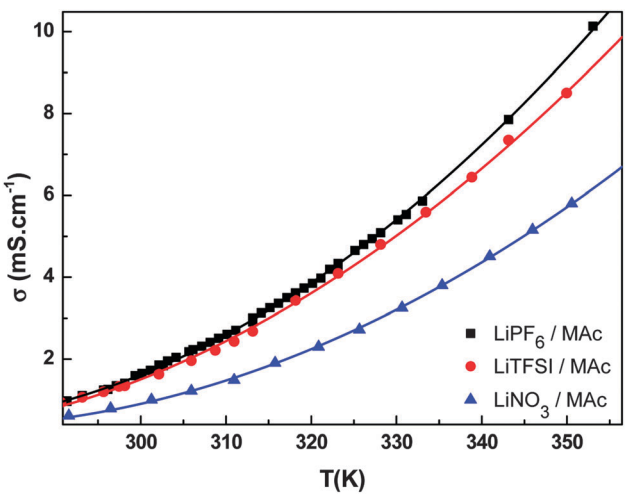

Fig. 3 Influence of temperature on the conductivity of the selected LiX–MAc mixture at x_{Li^+} = 0.20. The solid line serves as a guide to the eye.

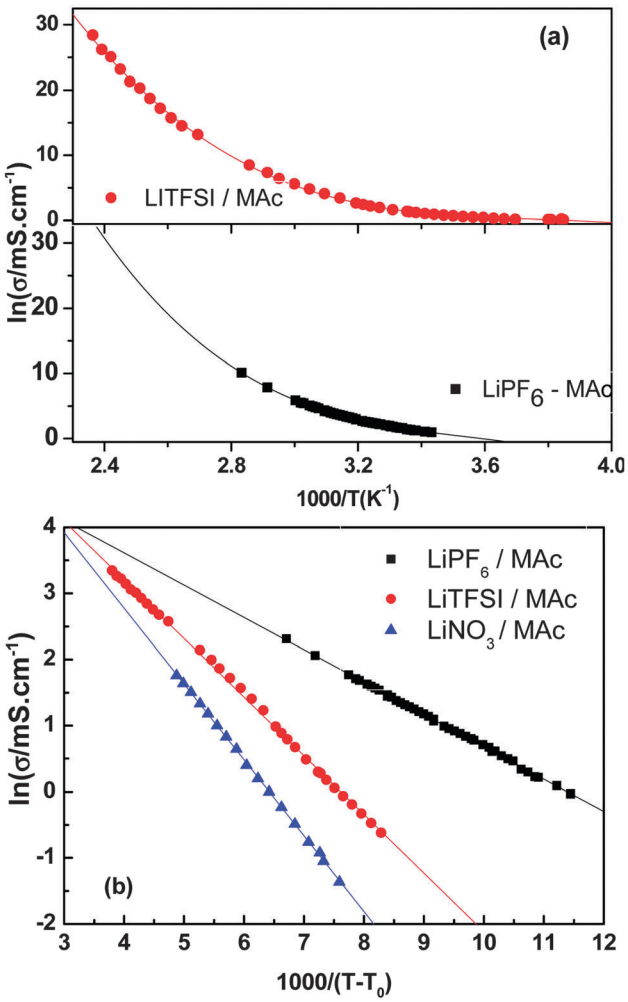

Fig. 4 Arrhenius (a) and VTF (b) plots describing the temperature dependencies on the ionic conductivity of selected LiTFSI–MAc and $LiPF_6$–MAc DES systems at x_{Li^+} = 0.20. The solid lines represent the Arrhenius or VTF fitting.

Table 3 VTF equation parameters for the conductivity and the viscosity (T_0, σ_0, η_0, B_1') of the DES LiX (X = $TFSI^-$, PF_6^- and NO_3^-)/MAc systems at x_{Li^+} = 0.20

Conductivity	T_0/K	σ_0/mS cm^{-1}	B/K	$R^{2\,a}$
LiTFSI–Mac	164	784	852	0.9994
$LiNO_3$–Mac	146	1587	1147	0.9997
$LiPF_6$–Mac	204	254	487	0.9991
Viscosity	T_0/K	η_0/mPa s	B'/K	$R^{2\,a}$
LiTFSI–Mac	160	0.253	807	0.9997
$LiNO_3$–Mac	158	0.085	1054	0.9990
$LiPF_6$–Mac	204	0.240	660	0.9975

[a] Correlation coefficient.

Viscosity. The viscosity has a strong effect on the rate of mass transport within the solution, which explains why the viscosity

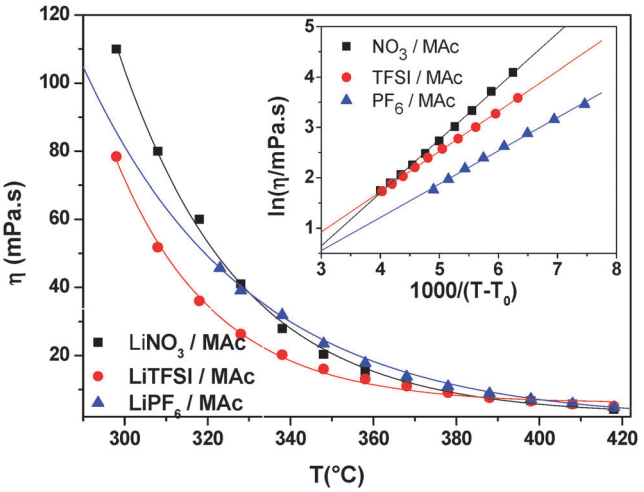

Fig. 5 Influence of temperature on the viscosity of DES systems LiTFSI–MAc, $LiPF_6$–MAc and $LiNO_3$–MAc at $x_{Li^+} = 0.20$. In the inset, the solid lines represent the VTF fitting.

is an important parameter for electrochemical studies. The viscosity can be influenced by several parameters such as the anionic species, their alkalinity, size, relative capacity to form hydrogen bonds, van der Waals interactions and size of the cation.[46,47] In the present work, the viscosity of the three studied systems ranges from 80 to 110 mPa s at 25 °C (see Table 2). A similar DES system based on LITFSI and acetamide has previously been reported to present a viscosity close to 110–150 mPa s, at 25 °C,[44,45] which is higher than viscosity values reported in the case of protic ionic liquids (PILs) based on the TFSI anion with the pyrrolidinium cation (η range from 55 to 95 mPa s at 25 °C), for example,[48] but these DES viscosity values seem to be closer to those reported in the case of the imidazolium-based PILs with the TFSI anion (η range from 90 to 117 mPa s at 25 °C).[49]

As expected, and shown in Fig. 5, the viscosity of each DES mixtures decreases as the temperature increases from 20 °C to 80 °C. This strong decreasing effect is due to the higher mobility of ions when the hydrogen bonds are broken. The viscosity is essentially attributed to the intermolecular hydrogen bonding (N–H···O) in MAc, which can be affected by an increase intemperature. An increase in temperature reduces then micro-domains created by the strong interactions described above which led to the formation of complexes between the majority of the MAc molecules, but maintains MAc–ion bonds.

The VTF equation (eqn (3)) was used to represent the temperature dependence of the viscosity of investigated DES.

$$\eta = \eta_0 \exp\left[\frac{-B_2'}{T - T_0}\right] \qquad (3)$$

Here, η_0 (mPa s), B_2' (K) and T_0 (K) are fitting parameters, and the ($B'R$) is a pseudo-activation in kJ mol^{-1}. According to eqn (3), fitting parameters can be determined for all studied systems from linear regression of $\ln(\eta)$ as a function of $(T - T_0)^{-1}$ as presented in the inset in Fig. 5, with the fitting parameters reported in Table 3. Each VTF-type fitting parameter is compared with those already reported in the case of the temperature dependence of the ionic conductivity of selected DES solutions. First, one can observe that, in the case of the $LiPF_6$–MAc, the fitted temperature T_0 is similar by fitting the temperature dependence of the conductivity and the viscosity, and reaches T_0 = 204 K. Secondly, in the case of the $LiPF_6$–MAc or the LiTFSI–MAc system, the parameter B', which is related to the pseudo-activation energy, is in similar magnitude calculated by using the VTF equation for the viscosity and for the conductivity as a function of temperature. It is notable that for the $LiNO_3$ based DES, this B' value is higher, which means that the variation of the viscosity is amplified with temperature. These later observations are in favor of the lithium ion diffusion especially at high temperature and suggest that these DESs can be suitable to be used as electrolytes for LiBs. Because each investigated LiX–MAc solution with a salt molar ratio close to 1/4 (*e.g.* $x_{Li^+} = 0.20$) possesses a melting temperature, close to the eutectic temperature, below the room temperature, (or stable surfusion phenomenon) and good transport properties, this ratio is chosen to evaluate then the electrochemical properties of LiX–MAc DES systems as electrolytes for LiB applications.

3.2. Electrochemical study

3.2.1. Electrochemical windows of DES. The electrochemical stability windows (ESWs) of three DESs-based electrolytes were studied by sweep linear voltammetry. We then decided to characterize the two systems based on the $TFSI^-$ and NO_3^- anions because they present different properties (like different electrochemical stability, affinity with water, *etc.*) while the PF_6^- based electrolyte present electrochemical properties close to those reported to the $TFSI^-$. Fig. 6 shows ESWs of LiTFSI–MAc and of $LiNO_3$–MAc at 20 °C. From Fig. 6, it appears that an oxidation wall is observed at 4.7 V and at 5.3 V for LiTFSI–MAc and $LiNO_3$–MAc, respectively. Therefore, by considering current

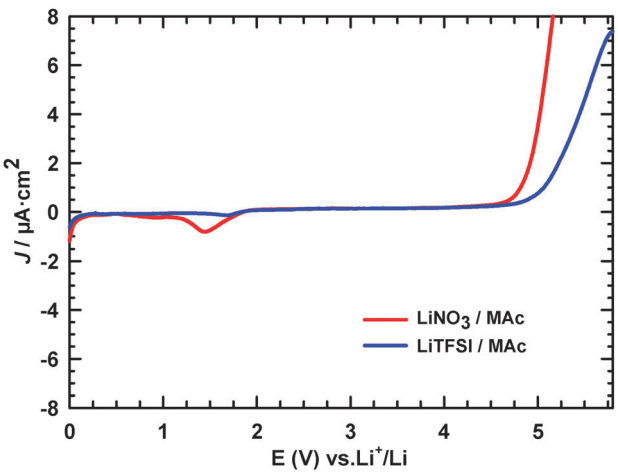

Fig. 6 Electrochemical stability window of LiTFSI–MAc and $LiNO_3$–MAc electrolytes at $x_{Li^+} = 0.20$ with platinum as the working electrode and Li as the reference and counter electrodes, scan rate = 10 mV s^{-1}.

density less than 0.01 mA cm^{-2}, the electrochemical stability window of these DESs on Pt is close to 4.7 to 5.3 V, respectively. The irreversible and small peak observed in reduction in the case of the $LiNO_3$ based system, at 1.2 V *vs.* Li^+/Li, could be attributed to the presence of water (around 600 ppm).

The cathodic limit showed by these electrolytes was significantly higher, comparable to that observed for ionic liquid. Furthermore, the anodic limit was comparable to electrolytes containing the NO_3^- and $TFSI^-$ anions. Considering these results, each DES appears to display an ESW large enough to be used as an electrolyte for LIBs. Nevertheless, due to the limited cathodic stability of these electrolytes in the presence of residual water, only anodic materials in which the insertion–extraction process of lithium occurs at potential higher than 1.2 V *vs.* Li/Li^+ can be considered to be suitable for use in DESs formulated in this study.

3.2.2. Cycling tests at room temperature. The electrochemical behavior of $LiFePO_4$ in lithium non-aqueous lithium electrolytes is widely reported in the literature.[50–54] In this media, the electrochemical reaction of $LiFePO_4$ is generally represented as $LiFePO_4 \leftrightarrows FePO_4 + Li^+ + e^-$, which means that the diffusion of lithium ions and the kinetics of electron transfer are the two key parameters which determine the performance of the cells. Fig. 7 summarizes typical constant-current charge–discharge behavior in the 100th cycle of $LiFePO_4$ in DES used as an electrolyte, herein using the LiTFSI–MAc solution as an example at a salt mole fraction of $x_{Li^+} = 0.20$ at two different water contents to understand the effect of residual water on the electrochemical behavior of selected DESs.

As shown, the $LiFePO_4$ electrode displays the typical voltage profile, and the plateau corresponding to the lithium insertion–extraction at around 3.45 V *vs.* Li/Li^+ and the difference between the charge and the discharge voltage plateau is relatively small. Obviously, the presence of water affects the specific capacity of the electrode and the lower the water content the higher the capacity. Nevertheless, the presence of different amounts of water does not seem to have an important effect on the voltage plateau.

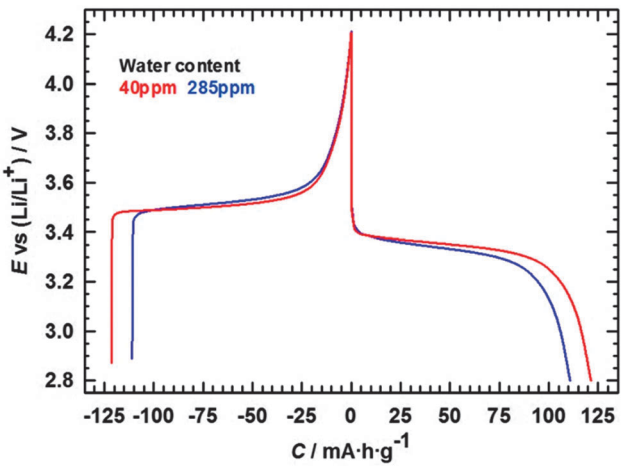

Fig. 7 Constant-current charge–discharge profiles of positive electrodes in LiTFSI–MAc at a $x_{Li^+} = 0.20$ electrolyte presenting a water content close to 40 ppm (red curve) and 285 ppm (blue curve) at the $LiFePO_4$ electrode. Current density: 0.02 mA cm^{-2}, cut-off: 2.8–4.2 V *vs.* Li/Li^+.

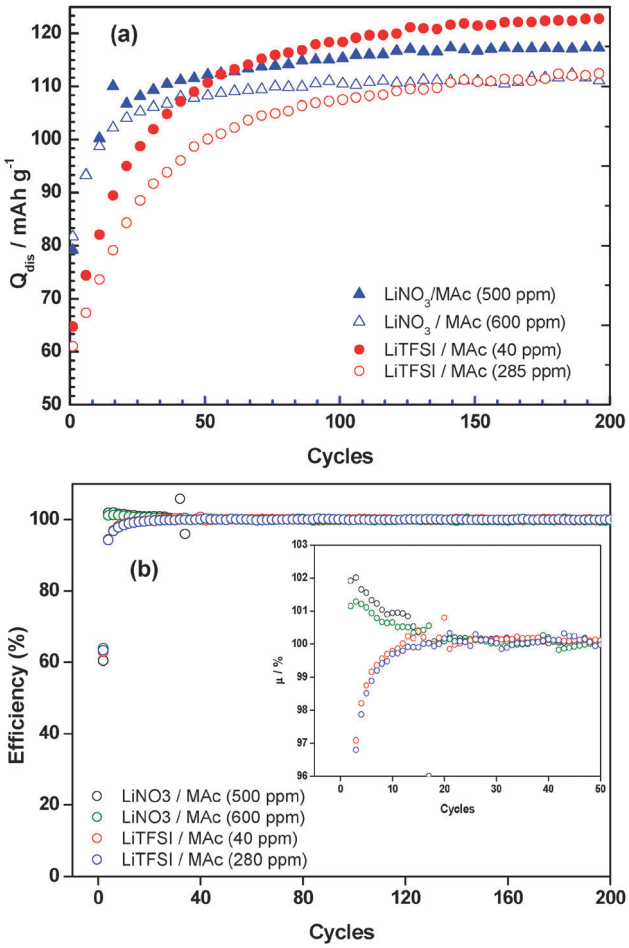

Fig. 8 Charge–discharge capacity (a) and efficiency (b) of LFP as obtained during tests carried-out at a 1 C rate in LiTFSI–MAc or $LiNO_3$–MAc electrolytes for two different water contents, at 25 °C.

Fig. 8 shows the plots of discharge capacities and efficiency of $LiFePO_4$ in LiTFSI–MAc and $LiNO_3$–MAc with different water contents (over 200 cycles). As shown, during the cycling the capacities in both electrolytes slowly increase. Most likely, since the two electrolytes are quite viscous, the observed behavior is due to an improvement in the wetting over the cycles. This kind of behavior has been observed in many IL-based electrolytes at room temperature and it is therefore not surprising. After 100 cycles, the discharge capacities stabilize, and the efficiency reaches values close to 99.9%. At 25 °C, the viscosity of DES is close to 100 mPa s, *i.e.* 35 times higher than conventional organic electrolytes based on mixtures of lithium salt and alkyl carbonates (for example, EC/DMC + 1 M LiTFSI has a $\eta = 3$ mPa s at 25 °C).[55] This observation suggests that the relatively low capacities in DES electrolytes are the result of the low level of electrolyte immersion into porous electrodes. Furthermore, the effect of water on the reversible capacity (Fig. 8a) seems to be obvious for both electrolytes. It is likely that the presence of small amounts of non-free water does not harm the cycle life but

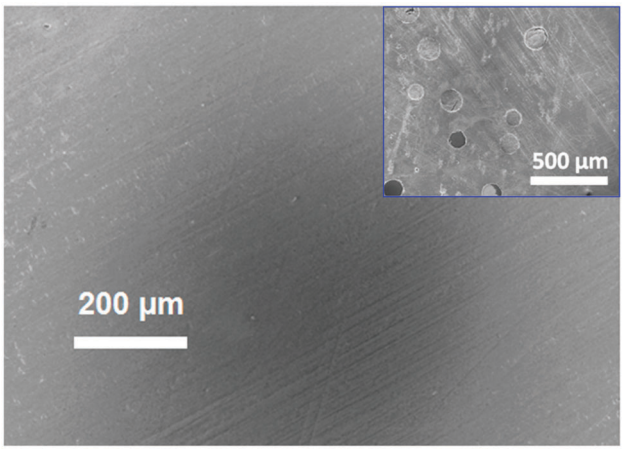

Fig. 9 SEM images of aluminum current collectors after cycling in LiTFSI–MAc at x_{Li^+} = 0.20, inset: after cycling in 0.3 M LiTFSI in PC.[57]

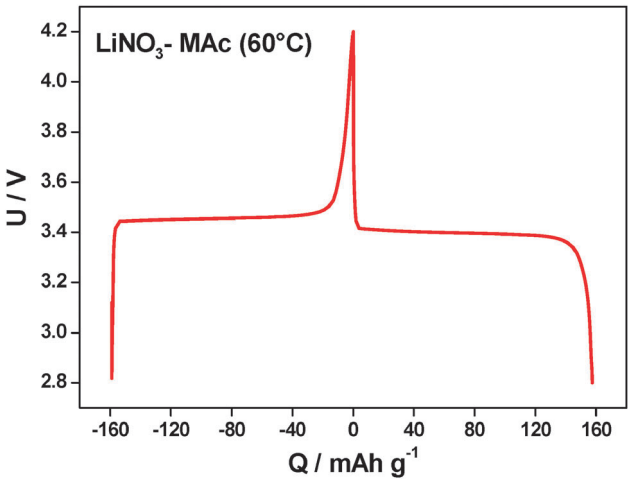

Fig. 10 Cycling curves obtained for $LiFePO_4$ cells in the 2.8–4.2 V *vs.* Li^+/Li voltage, at a 1 C rate and at 60 °C.

does not allow for maximum extraction–insertion of lithium of the LFP cathode.

3.2.3. Behavior of aluminum in DES electrolytes. Although LiTFSI has a high thermal stability and fine tolerance to water and is an outstanding candidate as salt for electrolyte formulation, there is an urgent need to control its effect on aluminum corrosion. Indeed, an aluminum electrode used as a positive electrode current collector corroded around 3.8 V *vs.* Li/Li^+ when the LiTFSI electrolyte was contained in LIBs.[56] Therefore, we investigate the behaviour of Al current collectors in the LiTFSI–MAc DES electrolyte. Fig. 9 shows SEM images of a current collector in aluminum of the LFP electrode cycled in a cell containing LiTFSI–MAc at x_{Li^+} = 0.20 taken at the end of the cycling at a 1 C rate and at 60 °C.

As shown in Fig. 9, the current collector cycled in LiTFSI-based DES displayed a quite uniform morphology, and only some residues were visible. By comparison in the inset was presented the collector cycled in 0.3 M LiTFSI in PC displaying holes of different size and depth, which were distributed all over the surface of the sample. As presented by Kühnel *et al.*, these holes were generated from the strong corrosion process occurring during the cycling in electrolytes containing the TFSI anion, which is able to solubilize $Al(TFSI)_3$ formed at the surface of the collector.[58] From these observations, it appears therefore evident that the LiTFSI–MAc DES based electrolyte displays the ability to prevent Al corrosion and can be considered to be a suitable electrolyte.

3.2.4. Temperature effects on cycling tests. Test cycling experiments were carried out at 60 °C in the 2.8–4.2 V *vs.* Li^+/Li voltage window to study possible changes in the electrochemical behavior and the redox kinetics in LFP.

Fig. 10 shows the charge–discharge profile (1st cycle) of $LiFePO_4$ in $LiNO_3$–MAc at x_{Li^+} = 0.20, as obtained at a 1 C rate and at 60 °C. As a consequence of increased conductivities at higher temperature, the irreversible capacity and the voltage difference between charge and discharge plateaus are slightly smaller than those observed at room temperature. By increasing the temperature, we do not observe either the diffusion effect on the material porosity as observed above at 25 °C in Fig. 8a. From this result, as expected, it is evident that the viscosity decreases (22–30 mPa s at 60 °C rather than 78–108 mPa s observed at 25 °C) with the temperature improving the wettability of the electrolyte with the $LiFePO_4$ electrode.

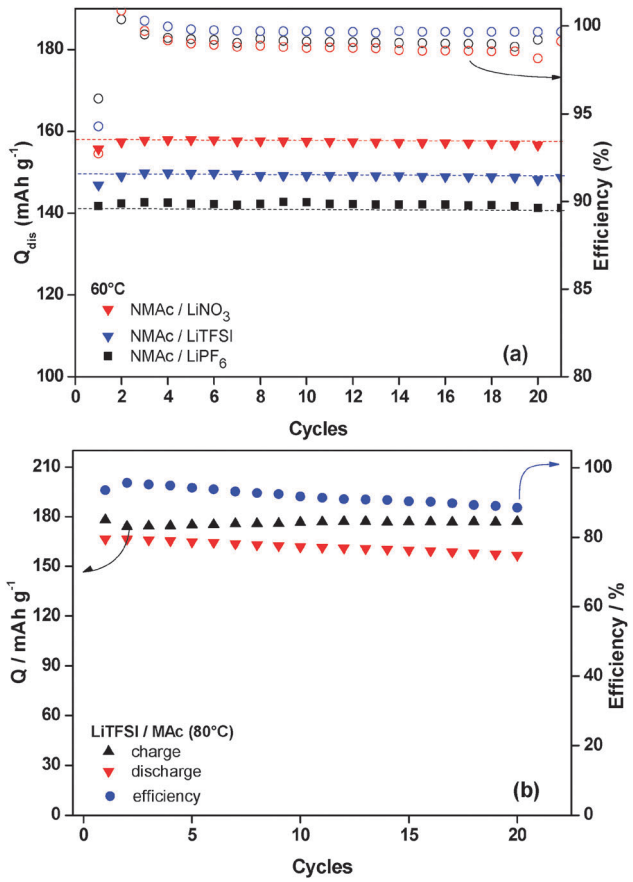

Fig. 11 Comparative discharge capacity and efficiency of LFP as obtained during tests carried-out at a 1 C rate containing (a) LiTFSI–MAc, $LiNO_3$–MAc, or $LiPF_6$–MAc at x_{Li^+} = 0.20 as electrolytes at 60 °C. (b) LiTFSI–MAc at x_{Li^+} = 0.20 as an electrolyte at 80 °C.

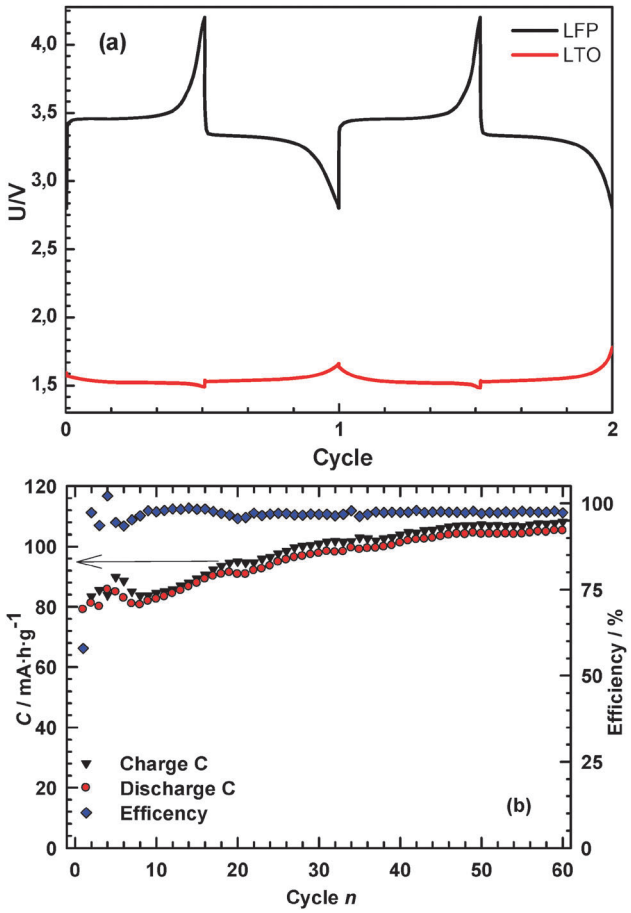

Fig. 12 (a) Charge–discharge voltage profiles of a LFP cathode and a LTO anode and (b) evolution of the discharge capacity and efficiency *vs.* cycle number for LIBs containing LiTFSI–MAc at x_{Li^+} = 0.20 as an electrolyte. The tests were carried out at RT at a 1 C rate.

The tests at 60 °C were carried out using the three investigated DES electrolytes and the results of these tests are reported in Fig. 11(a). As shown, during these tests the $LiFePO_4$ electrodes discharge display capacity of around 160, 150, and 140 mA h g^{-1} for $LiNO_3$, LiTFSI and $LiPF_6$ based DES, respectively. The efficiency of the charge–discharge process was higher than 99% over 20 cycles.

Using the LiTFSI–MAc solution tests were carried out also at 80 °C. As shown in Fig. 11(b) when this high temperature was applied the $LiFePO_4$ delivered almost its theoretical capacity, but the efficiency of the charge–discharge process decreases. After 20 cycles only 90% of the discharge capacity of the 1st cycle was maintained. Such a decrease was probably caused by the residual water present in the electrolyte.

Finally, also LIBs containing LFP as a cathode and LTO as an anode were assembled and tested at room temperature in LiTFSI–MAc at x_{Li^+} = 0.20 as an electrolyte at a 1 C rate. As shown in Fig. 12, the capacity delivered by the LIB increased over cycling, and after 100 cycles the battery displayed a discharge capacity in the order of 100 mA h g^{-1}. Even if this value of capacity is lower than those observed in conventional organic electrolytes based on alkylcarbonates (*e.g.* 150 mA h g^{-1}), it is important to note that it is higher than those obtained with aprotic ionic liquids-based electrolytes (C < 120 mA h g^{-1}).[59,60] Moreover, good efficiency of the LIB seems to indicate that LiTFSI–MAc can be safely used in combination with LFP and LTO based electrodes.

4. Conclusions

In summary, this work reports on the formulation, characterization and the application of three novel deep eutectic solvents composed of LiTFSI, $LiNO_3$ or $LiPF_6$ in mixture with *N*-methylacetamide (MAc), as electrolytes for LiB applications. Both LiX salts and MAc are solids at room temperature, but their mixture remains liquid at temperature below room temperature for a salt molar ratio between 0.10 and 0.35, with eutectic temperature ranging from −52 °C to −75 °C according to the nature of the selected anion. At a LiX/MAc molar ratio of 1/4, equivalent to a salt mole fraction of x_{Li^+} = 0.20, the temperature dependence of the ionic conductivity and the viscosity indicates a good pair of parameters and could also be described by the VTF equation. Each DES appears to display a high ESW of about 4.7 to 5.3 V on Pt and demonstrates also passivating behavior toward the aluminum collector, which suggest that these DESs are suitable as electrolytes for LiBs. Finally, a test cell was constructed and tested using the selected DESs as electrolytes. Each DES-based electrolyte allows the realization of devices LFP/DES/LTO showing promising capacity. The performance of the investigated LIBs appears to be promising also at 60 °C and even at 80 °C. Further investigation is certainly required to extend claimed conclusions, however the results of this work clearly show that DESs can be successfully introduced into LIBs. Considering the beneficial properties especially the cost of these electrolytes, such introduction could represent an important contribution for the realization of safer and environmentally friendly LIBs.

Acknowledgements

This research was supported by the CEA Le Ripault and ADEME agency (PhD grant of A. Boisset). Many thanks to the University of Münster, the Ministry of Innovation, Science and Research of North Rhine-Westphalia (MIWF) for the financial support.

Notes and references

1 A. P. Abbott, G. Capper, D. L. Davies and R. K. Rasheed, *Inorg. Chem.*, 2004, **43**, 3447–3452.
2 A. P. Abbott, G. Capper, D. L. Davies and R. K. Rasheed, *Chem.–Eur. J.*, 2004, **10**, 3769–3774.
3 A. P. Abbott, G. Capper, D. L. Davies, R. K. Rasheed and V. Tambyrajah, *Chem. Commun.*, 2003, 70–71.
4 A. P. Abbott, D. Boothby, G. Capper, D. L. Davies and R. K. Rasheed, *J. Am. Chem. Soc.*, 2004, **126**, 9142–9147.
5 A. Boisset, J. Jacquemin and M. Anouti, *Electrochim. Acta*, 2013, **102**, 120–126.

6 J. Zielkiewicz, *J. Chem. Thermodyn.*, 2000, **32**, 55; M. J. Earle and K. R. Seddon, *Pure Appl. Chem.*, 2000, **72**, 1391–1398.
7 S. Z. E. Abedin and F. Endres, *Acc. Chem. Res.*, 2007, **40**, 1106–1113.
8 B. Tang, W. Bi, M. Tian and K. H. Row, *J. Chromatogr., B: Biomed. Appl.*, 2012, **904**, 1–21.
9 S. Park and R. J. Kazlauskas, *Curr. Opin. Biotechnol.*, 2003, **14**, 432–437.
10 X. Han and D. W. Armstrong, *Acc. Chem. Res.*, 2007, **40**, 1079–1086.
11 R. Liu, J. F. Liu, Y. G. Yin, X. L. Hu and G. B. Jiang, *Anal. Bioanal. Chem.*, 2009, **393**, 871–883.
12 J. T. Gorke, F. Srienc and R. J. Kazlauskas, *Chem. Commun.*, 2008, 1235–1237.
13 G. Imperato, E. Eibler, J. Niedermaier and B. Konig, *Chem. Commun.*, 2005, 1170–1172.
14 S. Gore, S. Baskaran and B. Koenig, *Green Chem.*, 2011, **13**, 1009–1013.
15 F. Ilgen and B. Konig, *Green Chem.*, 2009, **11**, 848–854.
16 A. P. Abbott, J. Collins, I. Dalrymple, R. C. Harris, R. Mistry, F. Qiu, J. Scheirer and W. R. Wise, *Aust. J. Chem.*, 2009, **62**, 341–347.
17 Q. Zhang, K. De Oliveira Vigier, S. Royer and F. Jerome, *Chem. Soc. Rev.*, 2012, **41**, 7108–7146; C. A. Nkuku and R. J. LeSuer, *J. Phys. Chem. B*, 2007, **111**, 13271–13277.
18 M. Figueiredo, C. Gomes, R. Costa, A. Martins, C. M. Pereira and F. Silva, *Electrochim. Acta*, 2009, **54**, 2630–2634.
19 H. R. Jhong, D. S. H. Wong, C. C. Wan, Y. Y. Wang and T. C. Wei, *Electrochem. Commun.*, 2009, **1**, 209–211.
20 R. B. Leron and M.-H. Li, *Thermochim. Acta*, 2012, **530**, 52–57.
21 R. B. Leron and M.-H. Li, *J. Chem. Thermodyn.*, 2012, **54**, 293–301.
22 R. B. Leron, D. S. H. Wong and M.-H. Li, *Fluid Phase Equilib.*, 2012, **335**, 32–38.
23 K. Shahbaz, S. Baroutian, F. S. Mjalli, M. A. Hashim and I. M. Alnashef, *Thermochim. Acta*, 2012, **527**, 59–66.
24 K. Shahbaz, F. S. Mjalli, M. A. Hashim and I. M. AlNashef, *Fluid Phase Equilib.*, 2012, **319**, 48–54.
25 S.-H. Wu, A. R. Caparanga, R. B. Leron and M.-H. Li, *Thermochim. Acta*, 2012, **544**, 1–5.
26 Y. S. Hu, H. Li, X. J. Huang and L. Q. Chen, *Electrochem. Commun.*, 2004, **6**, 28–32.
27 A. K. Padhi, K. S. Nanjundaswamy and J. B. Goodenough, *J. Electrochem. Soc.*, 1997, **144**, 1188–1194.
28 N. Iltchev, Y. Chen, S. Okada and J. I. Yamaki, *J. Power Sources*, 2003, 749; N. Iltchev, Y. Chen, S. Okada and J. I. Yamaki, *J. Power Sources*, 2003, **749**, 119–121.
29 M. Koltypin, D. Aurbach, L. Nazar and B. Ellis, *Electrochem. Solid-State Lett.*, 2007, **10**, A40–A44.
30 C. C. Chang, T. K. Chen, L. J. Her and G. T. K. Fey, *J. Electrochem. Soc.*, 2009, **156**, A828–A832.
31 C. C. Chang and T. K. Chen, *J. Power Sources*, 2009, **193**, 834–840.
32 S. Menne, R. S. Kühnel and A. Balducci, *Electrochim. Acta*, 2013, **90**, 641–648.
33 *Gaussian View 3.0*, I. S. Gaussian, Inc., Pittsburgh, USA, 2000–2003.
34 A. Schaefer, C. Huber and R. Ahlrichs, *J. Chem. Phys.*, 1994, **100**, 5829–5835.
35 R. Ahlrichs, *TURBOMOLE User's Manual: Version 5.7*, COSMOlogic GmbH & Co. KG, Leverkusen, Germany, 2004.
36 F. Eckert and A. Klamt, *Version C2.1.*, COSMOlogic GmbH & Co. KG, Leverkusen, Germany, 2006.
37 A. Klamt and F. Eckert, *Fluid Phase Equilib.*, 2000, **172**, 43–72.
38 N. Ab Manan, C. Hardacre, J. Jacquemin, D. W. Rooney and T. G. A. Youngs, *J. Chem. Eng. Data*, 2009, **54**, 2005–2022.
39 A. F. Diorio, E. Lippincott and L. Mandelkern, *Nature*, 1962, **195**, 1296–1297.
40 G. Berchiesi, *J. Mol. Liq.*, 1999, **83**, 271–276.
41 F. Abdulnur and K. Laki, *J. Biophys.*, 1979, **28**, 503–509.
42 R. J. Chen, F. Wu, H. Y. Liang, L. Li and B. Xu, *J. Electrochem. Soc.*, 2005, **152**, A1979–A1984.
43 R. J. Chen, F. Wu, L. Li, B. Xu, X. P. Qiu and S. Chen, *J. Phys. Chem. C*, 2007, **111**, 5184–5194.
44 R. J. Chen, F. Wu, B. Xu, L. Li, X. Qiu and S. Chen, *J. Electrochem. Soc.*, 2007, **154**, A703–A708.
45 Q. Li, X. Zuo, J. Liu, X. Xiao, D. Shu and J. Nan, *Electrochim. Acta*, 2011, **58**, 330–335.
46 D. R. McFarlane, J. Sun, J. Golding, P. Meakin and M. Forsyth, *Electrochim. Acta*, 2000, **45**, 1271–1278.
47 G.-h. Tao, L. He, N. Sun and Y. Kou, *Chem. Commun.*, 2005, 3562–3564.
48 S. Fang, Z. Zhang, Y. Jin, L. Yang, S.-i. Hirano, K. Tachibana and S. Katayama, *J. Power Sources*, 2011, **196**, 5637–5644.
49 L. S. Headley, P. Mukherjee, J. L. Anderson, R. F. Ding, M. Halder, D. W. Armstrong, X. Y. Song and J. W. Petrich, *J. Phys. Chem. A*, 2006, **110**, 9549–9554.
50 A. K. Padhi, K. S. Nanjundaswamy and J. B. Goodenough, *J. Electrochem. Soc.*, 1997, **144**, 1188–1194.
51 R. Kostecki and F. McLarnon, *Electrochem. Solid-State Lett.*, 2002, **5**, A164–A167.
52 M. Yonemura, A. Yamada, Y. Takei, N. Sonoyama and R. Kanno, *J. Electrochem. Soc.*, 2004, **151**, A1352–A1356.
53 A. Eftekhari, *J. Electrochem. Soc.*, 2004, **151**, 1816–1819.
54 R. Dominko, M. Bele, M. Gaberscek, M. Remskar, D. Hanzel, S. Pejovmik and J. Jamnik, *J. Electrochem. Soc.*, 2005, **152**, A607–A610.
55 M. Dahbi, F. Ghamouss, F. Tran-Van, D. Leordant and M. Anouti, *J. Power Sources*, 2011, **196**, 9743–9750.
56 H.-B. Han, S.-S. Zhou, D.-J. Zhang, S.-W. Feng, L.-F. Li, K. Liu, W.-F. Feng, J. Nie, H. Li, X.-J. Huang, M. Armand and Z.-B. Zhou, *J. Power Sources*, 2011, **196**, 3623–3632.
57 S. Menne, R.-S. Kühnel and A. Balducci, *Electrochim. Acta*, 2013, **90**, 641–648.
58 R.-S. Kühnel, M. Lübke, M. Winter, S. Passerini and A. Balducci, *J. Power Sources*, 2012, **214**, 178–184.
59 A. Balducci, S. S. Jeong, G. T. Kim, S. Passerini, M. Winter, M. Schmuck, G. B. Appetecchi, R. Marcilla, D. Mecerreyes, V. Barsukov, V. Khomenko, I. Cantero, I. De Meatza, M. Holzapfel and N. Tran, *J. Power Sources*, 2011, **196**, 9719–9730.
60 G. T. Kim, S. S. Jeong, M. Joost, E. Rocca, M. Winter, S. Passerini and A. Balducci, *J. Power Sources*, 2011, **196**, 2187–2194.